CENTRAL ASIAN JOURNAL OF MEDICAL AND NATURAL SCIENCES

Volume: 03 Issue: 06 | Nov-Dec 2022 ISSN: 2660-4159

http:// cajmns.centralasianstudies.org/index.php

SYNTHESIS OF POLYOXIDE CATALYSTS AND THEIR APPLICATION POSSIBILITY IN CATALYTIC CONVERSION OF METHANE

Khurshid M. Saidov[1], Nurali K. Mukhamadiev[2], Shuhrat M. Sayitkulov[1], Oybek M. Tursunkulov[3]

EMAIL: xmsaidov@gmail.com, nuralimukhamadiev@gmail.com, oybtm09@gmail.com

Received 07th December 2022,
Accepted 25th December 2022,
Online 30nd December 2022

[1]Samarkand State University of Veterinary Medicine, Animal Husbandry and Biotechnology, M. Ulugbek Str., Samarkand 140110, Uzbekistan
[2]Samarkand state university, 15 University Boulevard, Samarkand 140110, Uzbekistan
[3]Center of Advanced Technologies under the Ministry of innovative development of the Republic of Uzbekistan, Talabalar shaharchasi street, 3A, 100174 Tashkent, Uzbekistan

ABSTRACT: The research is dedicated to the study of the conversion of methane with carbon dioxide using the catalysts containing NiO. The composites of oxides of the d-metals – catalysts that were prepared by the method of Solution-combustion synthesis using sol-gel technology is the object of the research. The morphology of the catalysts surface has been investigated by electronic microscopy (SEM), the phase composition by X-ray diffractometry (XRD), the element composition by X-ray microanalysis, the texture characteristics by McBen-Bakra mercury porometry. According to the results it was identified that the catalysts are high dispersed compounds, which composed of oxides of Ni, Al, Zr and Ti. The specific surface area of the polyoxide catalysts was determined to be SBET=420 ÷ 598 m2/g, the specific volume of the pores Vs=0,74 ÷ 0,92 cm3/g, the average diameter of pores D=220 ÷ 355 nm, the monolayer capacity am=1,5 ÷ 0,96 mole/kg and the adsorption saturation as =5,4 ÷ 2.2 moles/kg. Also, the catalytic activity of the catalysts was estimated by the carbonate conversion of methane. In this case the conversion of methane was 92%, carbon dioxide 87%, the yield of formed CO and H2 was 57,6 % and 51,9 % respectively.

KEYWORDS: catalyst, solution-combustion synthesis, composite, diffractometry, scanning electron microscopy, sorption, conversion, synthesis gas.

INTRODUCTION

The Republic of Uzbekistan is a country rich in natural gas, and according to the British Oil Company, the Statistical Review of World Energy and OPEC, it is among the top twenty countries in the ranking of the richest countries in gas (including shale gas) in 2018. More than 50 billion m^3 of natural gas is produced annually in Uzbekistan [1]. Most of the produced methane is used as a fuel for domestic consumption and exported. Only 1.5% of natural gas is processed [2].

It is known that natural gas serves as an important raw material for the production of hydrogen, ammonia, formaldehyde, methanol, diethyl ester, hyterocyclic compounds, ethylene and other products in chemical industry, and in Fisher –Tropsh synthesis [3]. Processing methane is the most perspective and optimal on economic site, because the price of the products like ethylene, formaldehyde, benzene prepared on the basis of "synthesis gas", which is formed as a result of catalytic conversion of methane - the main part of natural gas is 10÷100 times higher than that of raw materials [4].

All of the process of conversion of natural gas depends on the choice of catalysts used. Therefore, in the field of catalysis one of the priority direction is creation of a new generation catalysts and that requires to improve the preparation methods of them, to study the selective effects and activity of existing ones [5].

The synthesis method based on sol-gel technology for the preparation of composite catalysts and nanomaterials has been created at the end of the twentieth century. The synthesis is the method, which is based on high temperature and in this process the heat in a big amount is generated as a result of burning of metal nitrates (strong oxidants) and various reducing substances (flammable) and decomposition of metal nitrates [6,7,8]. Initially in the process of synthesis the powder of the reagents in a small size in the solution is formed. When the temperature reaches to 150-200℃, the process occurs throughout the entire volume and as a result a nanocomposite product is formed. The method is called "Solution-combustion synthesis". The method has a number of advantages comparing to other methods of synthesis including the solution of the initial substances allows them to mix in a molecular state, the increase of the temperature to 1000℃ in average ensures a high level of clean and crystallization of the powder particles. As the synthesis occurs in the short time and the formation of different gases in a big amount does not allow the particles getting bigger and lead to the formation of nanostructural powder with a high specific surface area [9,10,11].

The process of combustion and cooling occur at a high pace, and the formation of different intermediate and non-stoichiometric structural compounds creates many catalytic active centers. This method allows to prepare the catalysts and carriers with a geometric shape and size without additional treatment [12,13,14]. The main parameter of the process of synthesis of catalysts and carriers is a high combustion temperature. It in turn depends on the preparation process of the mixtures of initial substances, the synthesis conditions and the temperature of initial heating. Existence of organic and inorganic additives, which causes the gas to be generated in the initial mixture leads to form porosity and a high specific surface area in the catalysts synthesized [15,16].

Based on the above mentioned information, it should be noted that the method can be used to synthesize widely used nanomaterials, including catalysts, nanosorbents, nanoceramics, supercapacitors, optical materials, fuel cells, and products used in biotechnology [16,17]. From this perspective, the expansion of the nanomaterials synthesis sphere using and improving the method is one of the actual problems. Therefore, in this research using the "solution-combustion synthesis" method, the polyoxide catalysts based on some oxides of d-elements were synthesized, their physical-chemical characteristics studied and the application possibilities of them in catalytic conversion of methane evaluated [18,19,20].

EXPERIMENTAL SECTION

The following chemicals were used in the synthesis process: $Ni(NO_3)_2 \cdot 6H_2O$ chemically pure (99%), $ZrO(NO_3)_2 \cdot 2H_2O$ chemically pure (99,9%), $Ti(NO_3)_4$ chemically pure (98%), $Al(NO_3)_3 \cdot 9H_2O$ chemically pure (98%), $CO(NH_2)_2$ chemically pure (99,8%), $C_2H_5NO_2$ chemically pure (98,5%), HNO_3 chemically pure (98,5%).

The synthesis of the composites catalysts was carried out on the method of solution-combustion synthesis as follows: the masses of the chemical agents have been calculated for the preparation of their solutions or mixtures with different concentrations in distilled water at room temperature taking into

account the mutual reaction of the reagents. The saturated solutions of the initial substances were prepared taking into account the following dissolution values: $CO(NH_2)_2$=1.1 g/ml; $Ni(NO_3)_2$=3 g/ml; $Al(NO_3)_3$=0.85 g/ml; $ZrO(NO_3)_2$=0.3 g/ml; $Ti(NO_3)_4$ =0.3 g/ml. The mass of the reagents was weighed compared to 50 ml distilled water by analytical scale. The weighed samples of nitrates were completely dissolved in water trying to have it without precipitation [21]. Nitric acid was added to the solution to form an acidic environment in it. The solutions have been heated and thoroughly mixed with each other for complete saturation of them. To perform the reaction the mixture was heated using an electric heater up to maximum bounds. As a result of the solution boiling it began to turn into thick mass, which forms gas. After evaporation of a part of the distilled water, the solution turned into gel-like product. The gel began to burn spontaneously after the temperature raised up to the temperature of the combustion temperature of the gel. As a result, the product with small density and high porosity has been formed. The synthesis product has been grinded for about 10 minutes to get it with the same size. The sample has been calcined for 4 hours increasing the temperature of the oven from room temperature to 800℃ with the speed of the temperature 1-2℃/min and as a result a composite product was prepared. Figure 1 describes the scheme of the synthesis of composites catalysts using the method of solution-combustion synthesis [20,21].

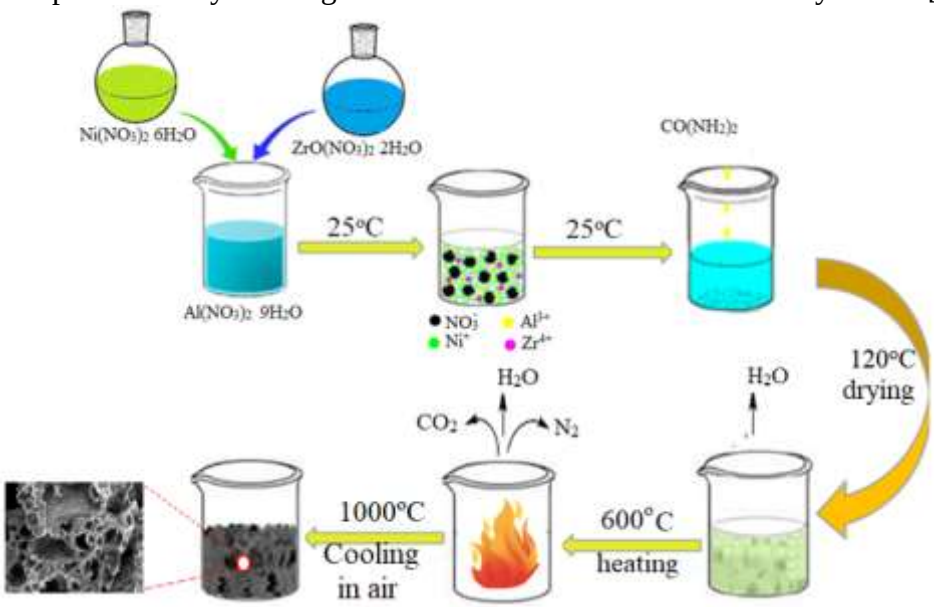

Figure 1. Scheme of the synthesis of the catalysts on the method of solution-combustion synthesis.

The X-ray phase analysis of the synthesized catalysts was studied by PANalytical Empyrean X-ray diffractometer (XRD) [22,23], the surface area morphology by scanning electron microscope SEM eVO MA 10 (Carl Zeiss) [24,29], the elemental analysis by SEM equipped with energy dispersion X-ray spectrometer (EDS Aztec Energy Advanted X-Act, Oxford Instruments). SEM-EDS was used as one of the reliable methods to determine the size and the main composition of the particles. Also the method allows to determine nano characteristics of the samples [26,27,28]. The sorption isotherm composed based on the results of the sorption of different substances vapors at low temperature on McBen-Bakra's sensitive spiral quartz device was used to determine the specific surface area of the catalysts, the average diameter of the pores, the volume and monolayer capacity of the pores [31,32,33].

The carbonate catalytic conversion of methane was conducted on a flow reactor. The central part of the reactor consists of quartz tube and the catalyst tablets were placed in its 50 mm part and both sides of that have been closed with glass fiber plug. To control the reaction temperature a thermocouple has been placed in the tube. The scheme of laboratory reactor is presented in Figure 2.

The temperature of the reactor was controlled by thermocouple and the exact amount of gases mixture was sent to it through pressure reducing valve from gas sources. The gases mixture was sent to the evaporating device to be purified from impurities, and then directed to the reactor. The gases passed through the reactor and the product prepared were passed through condenser. The composition of the reaction mixture has been identified by the method of gas chromatography.

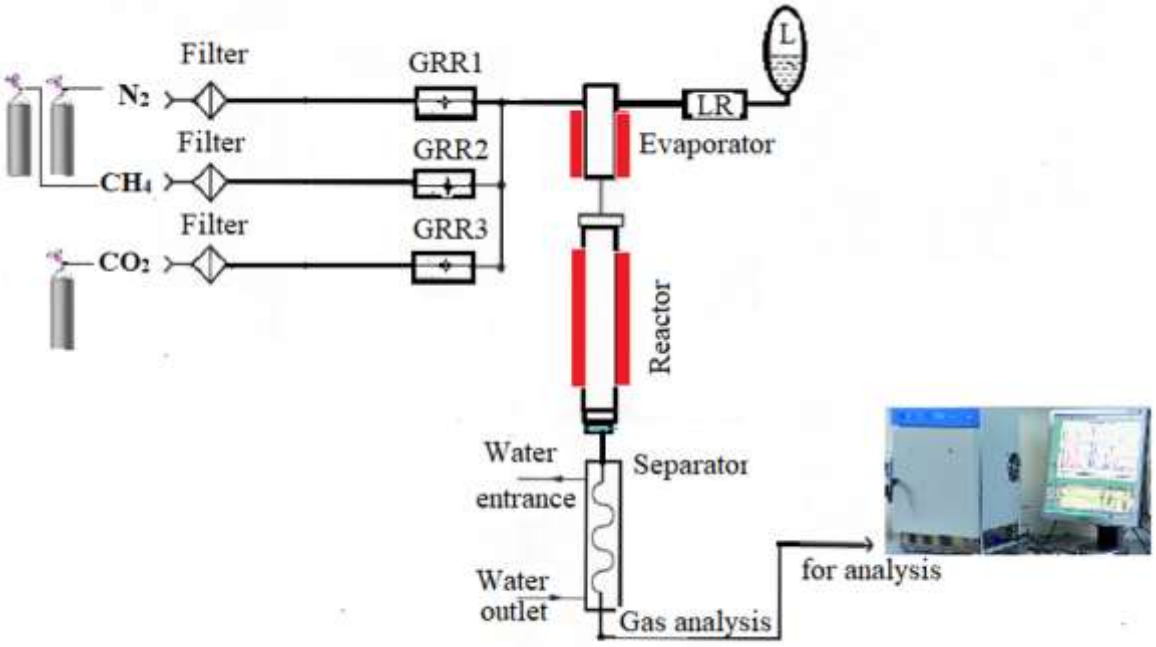

Figure 2. General scheme of the catalytic conversion process of methane.

To separate the components of the reaction mixture, a gas chromatograph with a capillary column 25 m long and 0.5 mm in inner diameter was used. Chromatograph allows to analyze H_2, O_2, CH_4, C_2H_6, C_2H_4, C_3-C_4 hydrocarbons, CO and CO_2 and many organic substances. In the analysis process the temperature of thermal conductivity detector was 260°C, the temperature of the evaporator - 280°C, the temperature of the column - 40°C. The speed of the carrier gas flow N_2 =30 ml/min. The mixtures of accurately measured pure samples or with the known concentration were sent to the chromatograph with a microsyringe and results were obtained.

RESULTS

3.1. Characterization of Catalysts

3.1.1. XRD and SEM Analysis

The X-ray phase analysis of the synthesized catalysts was studied by PANalytical Empyrean X-ray diffractometer (XRD Shimadzu). The parameters of the X-ray diffractometer were set up as follows: CuK_α–radiation (β–filter, Cu, 1,5406 A° current mode), the voltage - 30 kV, the intensity of current - 10-20 ampere. The intensity of diffracted X-rays was determined by superimposing waves emitted by different atoms in the same unit cell. The phase composition of the samples was analyzed by a semi-quantitative method based on calibration standards. The phases structures and diffraction patterns were compared with the data recorded on the database of the International Center for Diffraction Data (ICDD) and literatures.

It is known that in accordance with the above approach, the XRPhA gives results on the phase composition of the catalysts studied.

Initially, the phase composition of the catalyst synthesized from $Ni(NO_3)_2 \cdot 6H_2O$, $ZrO(NO_3)_2 \cdot 2H_2O$, $Al(NO_3)_3 \cdot 9H_2O$ and urea was analyzed by the X-ray phase method (Fig. 3). On the X-ray diffractogram, the spectrum output was observed at 2θ=19.06°, and the highest intensity was recorded at 2θ=37.10°. In addition, the spectrum output were also observed at 2θ = 44.99°, 2θ = 31.39°, 2θ = 59.67°, 2θ = 62.86°, 2θ = 65.57°, all of which are mostly filled with 3-phase compositions. In addition, 2nd = 44.99°, 2nd = 31.39°, 2nd = 59.67°, 2nd = 62.86°, 2nd = 65.57°, all of which are mostly filled with 3-phase compositions, we can foresee this. The crystal structure is predominantly cubic, the phase composition consists of nickel oxide (NiO), nickel aluminate ($NiAl_2O_4$) and zirconium oxide ($ZrO_{1,88}$). This is consistent with the information in the literature [34,35,36].

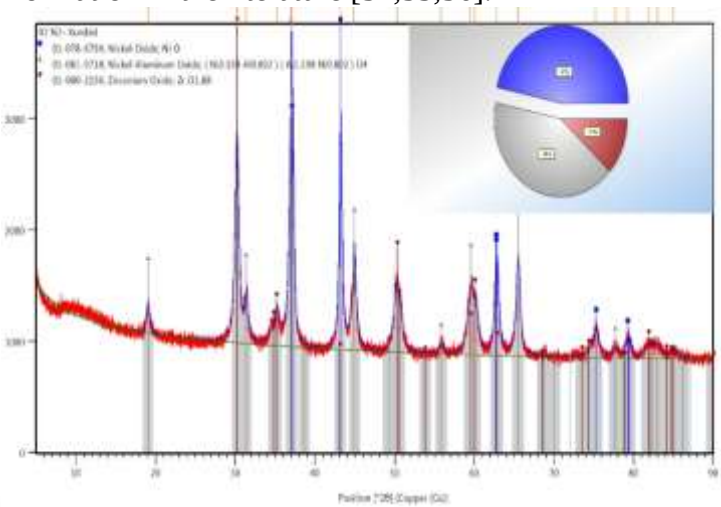

Figure 3. Diffractogram of K1 catalyst

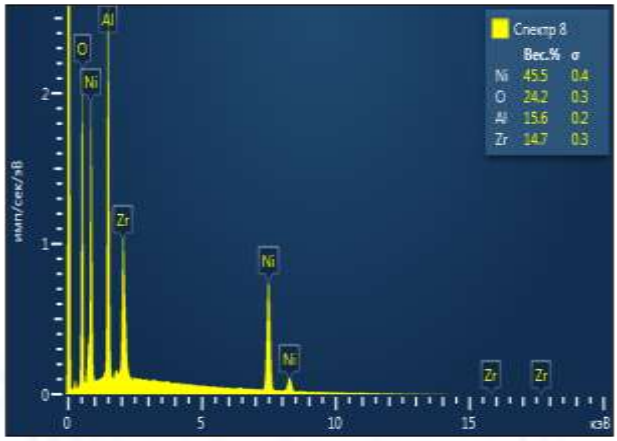

Figure 4. Element composition of K1 catalyst

At the same time, an elemental analysis was carried out using X-ray spectral microanalysis on the specified surface of the catalysts (Fig. 4). It showed us that according to the results of the analysis obtained from individual surface areas, the composition of the catalyst $NiO \cdot NiAl_2O_4 \cdot ZrO_{1.88}$ corresponds to the molar ratios of the initial reagents and that there are no other additional components in its composition.

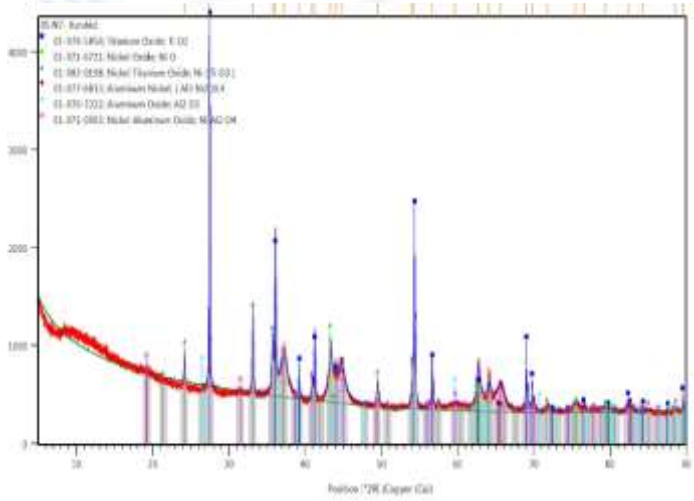

Figure 5. X-ray diffractogram of K2 catalyst

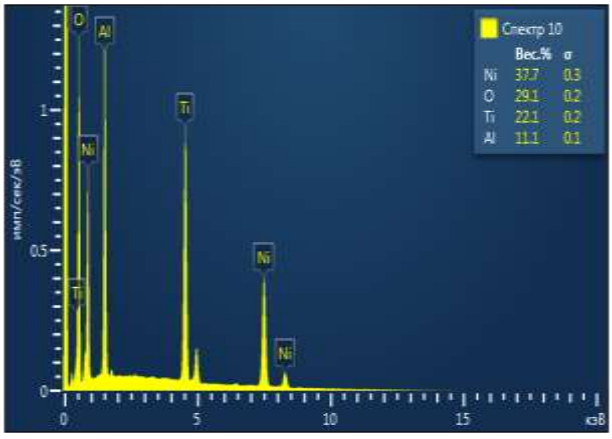

Figure 6. Element composition of K2 catalyst

When replacing the alloying impurity $ZrO(NO_3)_2 \cdot 2H_2O$ in the catalyst with $Ti(NO_3)_4$, its phase (Fig. 5) and elemental (Fig. 6) compositions were analyzed.

A number of changes in the phase composition of the sample were observed due to the alloying impurity. In particular, on the diffractogram, the spectrum output was observed at 2θ=24.21°, and the highest intensity was recorded at 2θ=27.50°. In addition, the high intensity of the spectra was also observed at 2θ =33.18°, 2θ =35.76°, 2θ =37.28°, 2θ =41.30°, 2θ =54.38°, 2θ =56.70°, 2θ =62.81°, 2θ =64.14°, 2θ =65.60°, 2θ =69.09°. It shows that, unlike the catalyst mentioned above, it consists of 6 phases. The crystal structure is mainly tetragonal, cubic and hexagonal and the correspondence of the phase composition to NiO, TiO_2, $NiTiO_3$, $Al_3Ni_2O_4$, Al_2O_3, $NiAl_2O_4$ was determined by the comparison with the data in the database of the International Center for Diffraction Data (ICDD). At the same time, it was confirmed that the main intense spectra belong to TiO_2 and that it exists in a crystalline state and corresponds to the literature data [37,38].

The results of the analysis of the elemental composition of individual surface areas showed that the ratio of elements in the catalyst containing NiO, TiO_2, $NiTiO_3$, $Al_3Ni_2O_4$, Al_2O_3 and $NiAl_2O_4$ corresponds to the ratio in the starting materials.

The degree of compatibility of the components of both catalysts can be judged by comparing the X-ray spectra (Fig. 7).

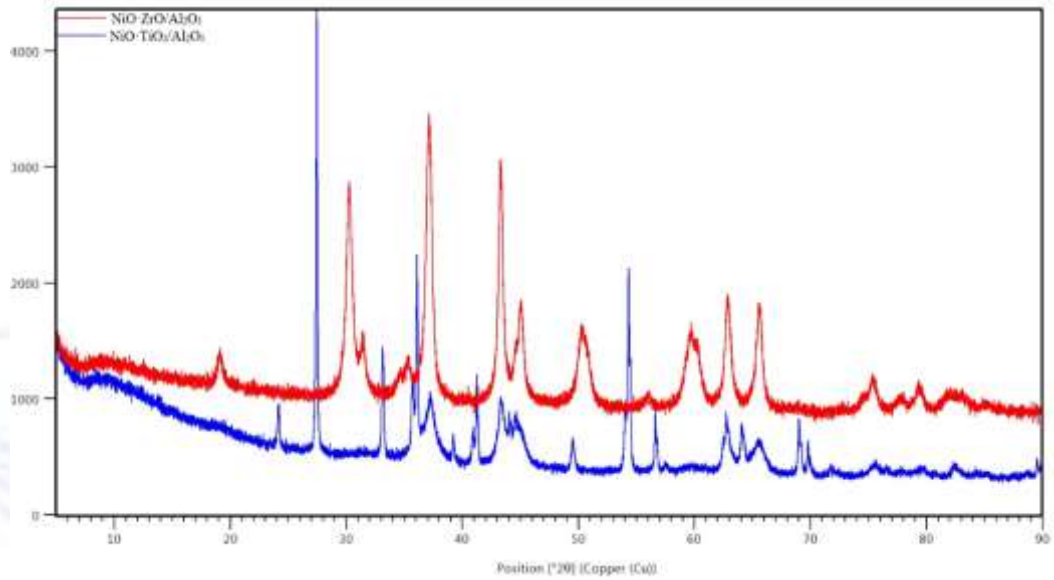

Figure 7. X-ray diffractogram of the composite catalysts K1 and K2.

When $ZrO(NO_3)_2 \cdot 2H_2O$ and $Ti(NO_3)_4$ are used together as dopants, the highest intensity was recorded on the X-ray diffractogram at 2θ=54.05° (Fig. 8). In addition, the output spectra are observed at 2θ=33.14°, 2θ=35.70°, 2θ=54.05°, 2θ=54.32°, 2θ=36.08°, 2θ=24.17°, 2θ=49.50°, 2θ=64.12°, 2θ=40.51°, 2θ=30.10°. At the same time, the crystal structure is mainly tetragonal, cubic and hexagonal, the phase composition corresponds to $NiTiO_3$, TiO_2, $ZrO_{1.99}$, $(Al_3Ni_2)_{0.4}$, $Al_{16}Ni_7Ti_6$ and $NiAl_3Zr_5$, and the presence of the phase compositions with the basic crystal structure of $NiTiO_3$ and TiO_2 can be noted.

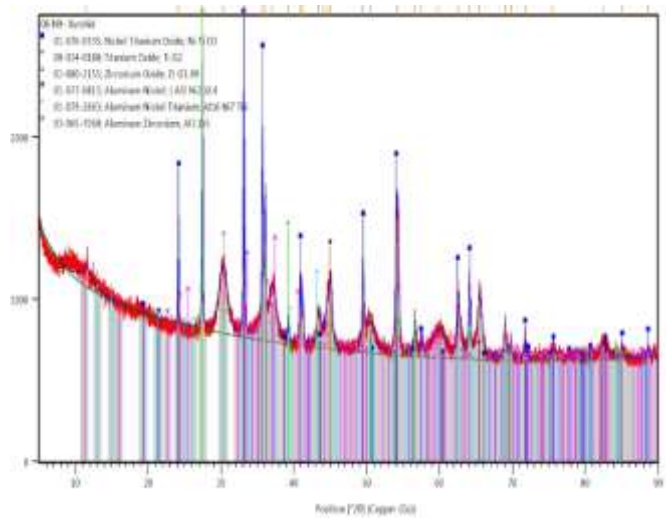

Figure 8. Diffractogram of K3 catalyst

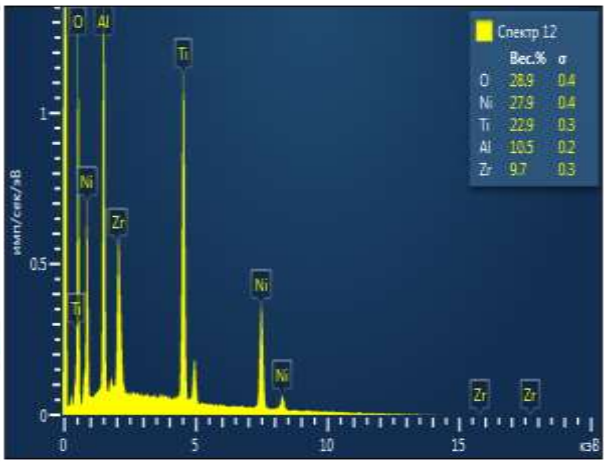

Figure 9. Element composition of K3 catalyst

The results of the analysis of the elemental composition of individual surface areas showed that the ratio of elements in the catalyst with the phase composition $NiTiO_3$, TiO_2, $ZrO_{1.99}$, $(Al_3Ni_2)_{0.4}$, $Al_{16}Ni_7Ti_6$ and $NiA_{l3}Zr_5$ corresponds to the ratio in the starting materials (Fig. 9).

The effect of the dopant introduced into the catalyst samples on the phase composition and the level of compatibility of the spectra has been shown (Fig. 10), and the formation of the same phase composition of TiO_2, $NiTiO_3$ in the catalysts K2 and K3 provides a close level of compatibility.

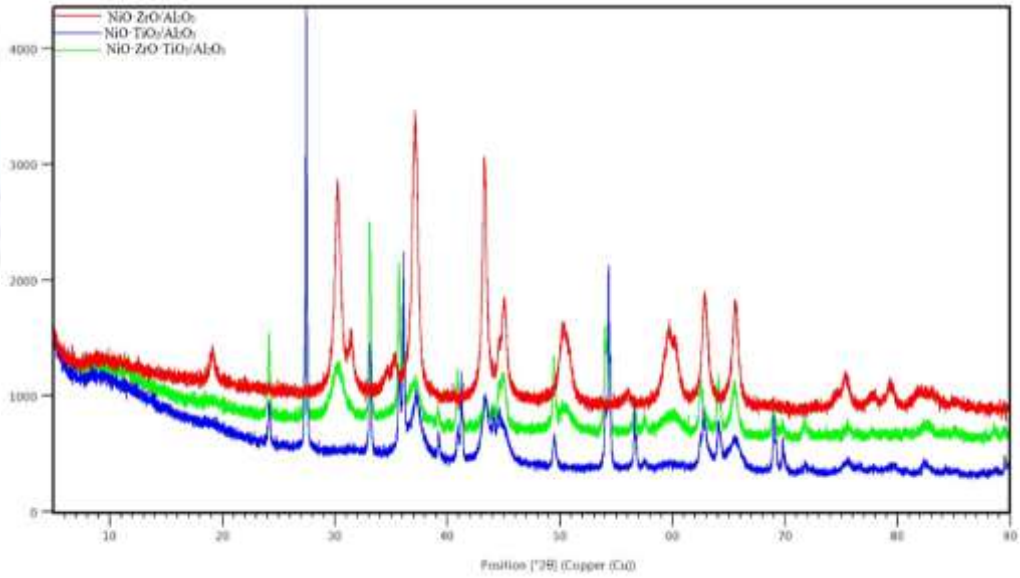

Figure 10. X-ray diffractogram of the composite catalysts K1, K2 and K3.

From the abovementioned information, the phase composition of the catalyst and the main phase composition were summarized (Table 1).

Table 1. The phase composition of the catalysts

Catalysts	Phase composition	Main phase composition
K1	$NiO{\cdot}NiAl_2O_4{\cdot}ZrO_{1.88}$	NiO, $ZrO_{1.88}$

K2	NiO, TiO_2, $NiTiO_3$, $Al_3Ni_2O_4$, Al_2O_3, $NiAl_2O_4$	$NiTiO_3$,TiO_2
K3	$NiTiO_3$, TiO_2, $ZrO_{1.99}$,$(Al_3Ni_2)_{0.4}$, $Al_{16}Ni_7Ti_6$, $NiAl_3Zr_5$	$NiTiO_3$,TiO_2, $ZrO_{1.99}$

The table shows that the phase composition of the catalysts is close and compatible with each other, and the phase composition of the catalysts K2 and K3 is different compared to K1. This indicates a good chemical interaction of the initial products in the synthesis process.

3.1.2. Sorption characteristics

It is known that the adsorption process takes place in the kinetics of heterogeneous catalytic reactions. Therefore, the study of the sorption characteristics of catalysts is an important characteristic of catalysts. Based on the abovementioned, the textural characteristics of the catalysts, such as specific surface area, pore size and average diameter were studied by adsorption of benzene and toluene vapors in a McBen-Bakra sensitive spiral quartz device (Fig. 11).

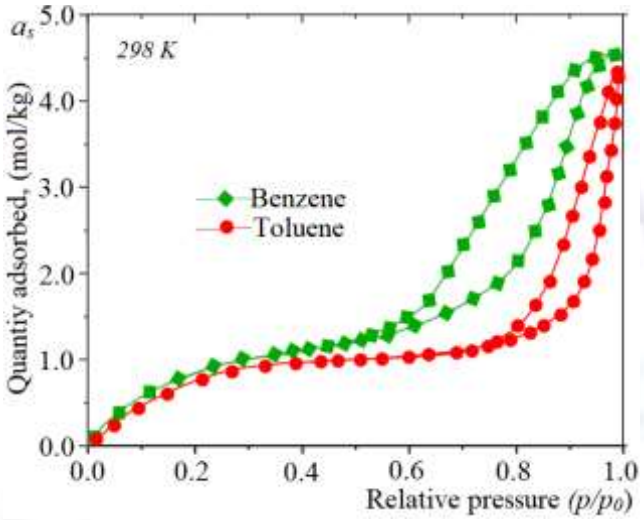

Figure 11. The adsorption isotherm of benzene and toluene steam

It can be seen from the sorption isotherms that the main amount of sorbed adsorbates falls in the range p/p_o = 0.1-0.4. Also, at a relative pressure p/p_o = 0.72-0.98, the hysteresis loops were formed due to capillary condensation in mesopores. The formation of hysteresis loops at high relative pressure showed that the catalyst consists of relatively large mesopores and macropores. This can be confirmed by the SEM image of the catalyst sample (Fig. 12a, b).

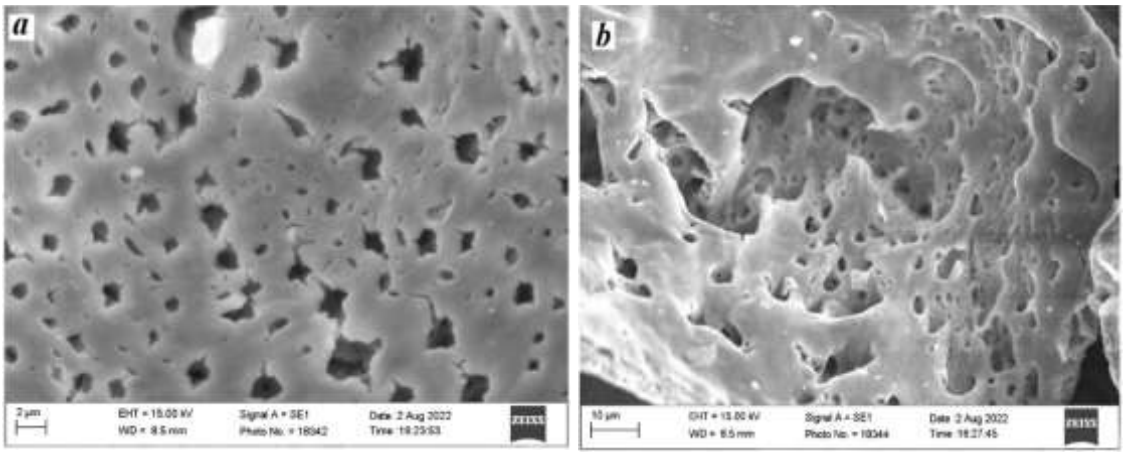

Figure 12 a,b. SEM image of K1 catalyst surface

It can be seen from the images that the pores are evenly distributed over the catalyst surface, and they are the same in size, that is, they are monodisperse. In Figure 12a, the pores on the surface and the pore size are the same and close to each other. We can see the arrangement in dimensions and the maximum porosity of the surface. In Fig. 12b the layer-by-layer arrangement of the pores on the surface of the catalyst and the porosity of the internal parts of the catalyst can be observed.

The sorption isotherms of benzene and toluene vapors on the K2 catalyst are shown in Fig.13. The figure shows that the adsorption isotherms sharply increase from zero relative pressure to p/p_o=0.6 and approach saturation at p/po=0.95. It is also seen that at a relative pressure p/p_o =0.6÷0.9 due to capillary condensation, the adsorption and desorption lines are connected, forming hysteresis loops. This indicates that the catalyst contains relatively large mesopores. The calculations showed that 60.5% of the total number of catalyst pores are macropores, and 39.5% are mesopores.

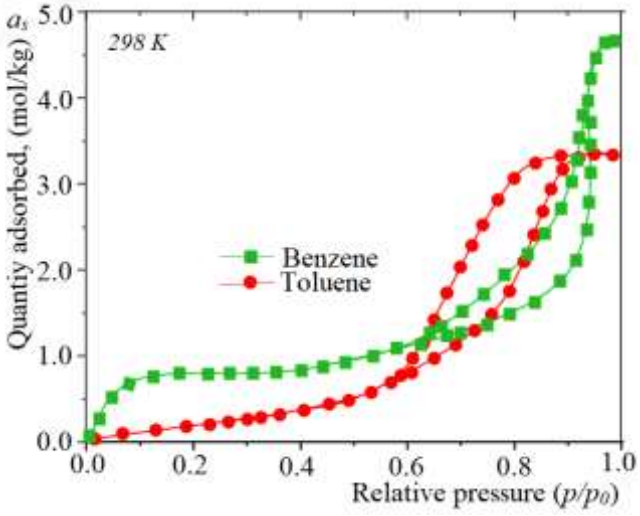

Figure 13. Sorption isotherms of benzene and toluene vapors

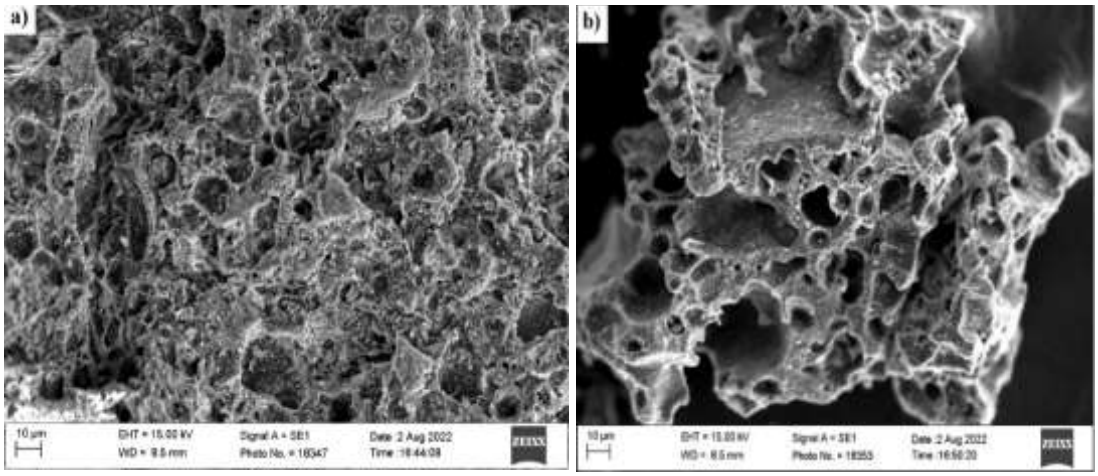

Figure 14 a,b. SEM image of the surface of K2 catalyst

Fig. 14a shows that there are many pores on the surface of catalyst K2, as in catalyst K1, and the pores of the same size and shape can be seen in Fig. 14b.

The process of sorption of benzene and toluene vapors was also studied on catalyst K3, and sorption isotherms were obtained. The isotherms showed saturation of macropores with a sharp increase in relative pressure up to p/p_o=0.5 and saturation of mesopores in the range of p/p_o=0.2÷0.5. Adsorbed vapors of benzene and toluene formed hysteresis loops by merging adsorption and desorption lines in the range of relative pressures p/p_o=0.5÷0.8 due to capillary condensation. Data found using adsorption isotherms showed that 74.3% of the total pores of the catalyst are macropores, and 25.7% are mesopores.

It has been established that the adsorption isotherms of benzene and toluene vapors on a catalyst containing Al_2O_3, $NiAl_2O_4$, $NiTiO_3$, TiO_2, $ZrO_{1.99}$, $(Al_3Ni_2)_{0.4}$, $Al_{16}Ni_7Ti_6$, $NiAl_3Zr_5$, obtained by the solution combustion reaction belong to type V according to the IUPAC classification (Figure 15).

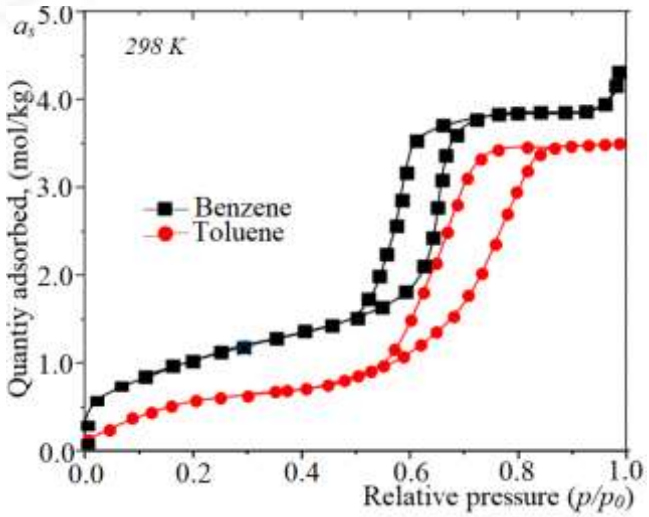

Figure 15. Sorption isotherm of the vapors of benzene and toluene on catalyst K3

On the surface of catalyst K3, as in above mentioned catalysts the uniformly distributed porosity and overlapping of the pores over the entire surface can be observed. In Fig. 16a shows a uniform distribution of the pores on the catalyst surface, the location of the pores on the surface, and the pore sizes in the same, close to each other sizes. Fig. 16b shows the presence of macropores and mesopores on the catalyst surface.

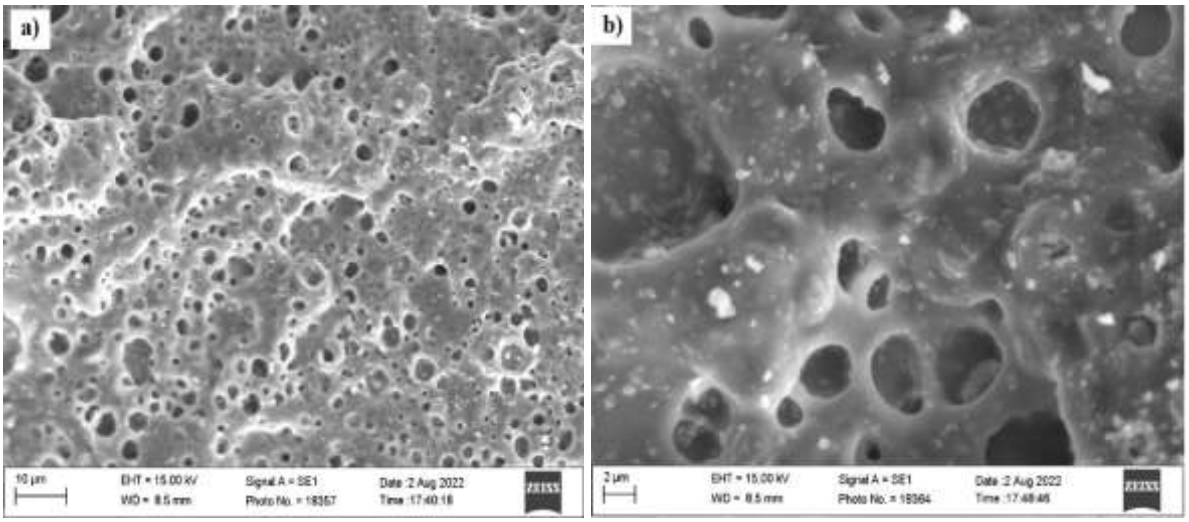

Figure 16 ***a,b.*** SEM image of the surface of K3 catalyst

Based on the results of sorption isotherms and SEM, the specific surface area of the catalysts (S_{BET}, m^2/g), average pore diameter (D, nm), capacity of the sorbent monolayer (a_m, mol/kg), and adsorption saturation (a_s, mol/kg) were determined (Table 2).

It can be seen from the table that the specific surface area of catalyst K3 prepared with the combined use of dopants S_{BET} = 598.0 ± 17.4 m^2/g is large, and the pore size is small 220.0 ± 15.7 nm, respectively, respectively the other parameters too. It is noted that these textural characteristics decrease from K1 to K2 and increase to K3. This can be explained by the relatively large number of meso- and macropores on the surface of catalyst K3 than that of K1 and K2.

Table 2. Texture Characteristics of the Catalysts

n	Initial Substances	Phase composition	V_s, cm^3/g	a_m, mol/kg	S_{BET}, m^2/g	a_s, mol/kg	D, nm
K1	$Ni(NO_3)_2 \cdot 6H_2O$ $ZrO(NO_3)_2 \cdot 2H_2O$ $Al(NO_3)_3 \cdot 9H_2O$, $C_2H_5NO_2$, HNO_3	NiO, $NiAl_2O_4$, $ZrO_{1.88}$	0.86±0.04	1.10 ±0.02	510.2±25.2	4.2±0.8	284.0±16.3
K2	$Ni(NO_3)_2 \cdot 6H_2O$, $Ti(NO_3)_4$, $Al(NO_3)_3 \cdot 9H_2O$, $CO(NH_2)_2$, HNO_3	NiO, $Al_3Ni_2O_4$, TiO_2, $NiTiO_3$, Al_2O_3, $NiAl_2O_4$	0.74±0.05	0.96 ±0.01	420.4±12.6	22.0±0.4	355.0±18.5

K3	$Ni(NO_3)_2 \cdot 6H_2O$, $ZrO(NO_3)_2 \cdot 2H_2O$, $Al(NO_3)_3 \cdot 9H_2O$, $Ti(NO_3)_4$, HNO_3 $CO(NH_2)_2$	$NiTiO_3$, TiO_2, $ZrO_{1.99}$, $(Al_3Ni_2)_{0.4}$, $Al_{16}Ni_7Ti_6$, $NiAl_3Zr_5$	0.92±0,02	1.50±0,04	598.0±17.4	5.4±0.3	220.0±15.7

3.2. Application of polyoxide catalysts in methane conversion

Using these synthesized catalysts in the carbonate conversion of methane, the catalytic activity in this process was studied. The effect of the reaction temperature on the catalytic activity of the catalysts and volume velocity on the process, as well as coking of the catalyst surface after conversion, has been studied [38,39,40] and found to be consistent with these literatures.

First, the effect of volume rate on the catalytic activity of the catalysts in the range of 1500-15000 h^{-1} was studied. The reaction process was carried out in a quartz tubular flow reactor in the range of 700-900 ℃, the volume flow rate of gas mixtures (CH_4:CO_2:N_2 20:20:60) was 100 cm^3/min [41.42, 43.44] and according to the literature data were results close to the data were obtained.

The catalytic conversion of methane depends on temperature, with an increase in temperature, the efficiency of methane conversion in percent increases, as a result of which it can be seen that the efficiency of gas formation is also high (Fig. 17).

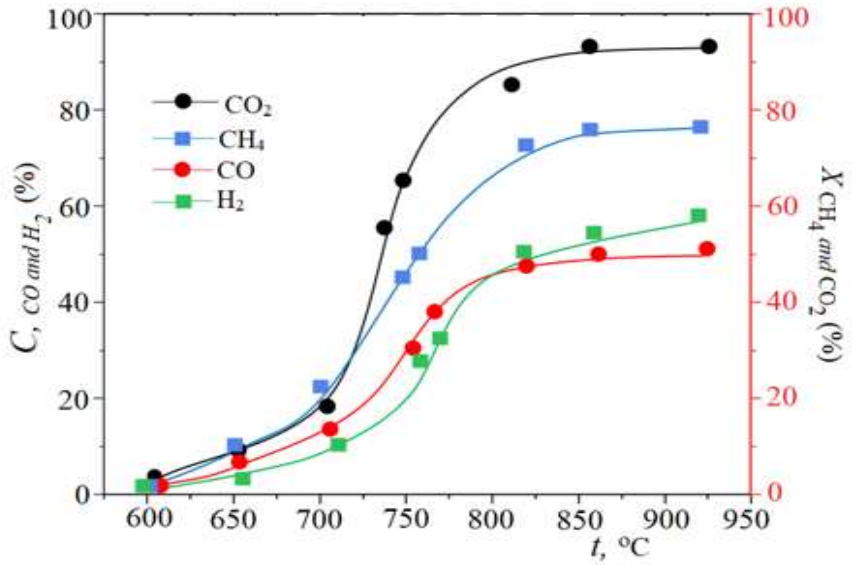

Figure 17. Effect of the reaction temperature on the carbonate conversion and the concentration of the main conversion products: 1 - CO_2, 2 - CH_4, 3 - H_2 and 4 - CO

Figure 17 shows the effect of the reaction temperature on the carbonate conversion and the concentration of the main conversion products: 1 - CO_2, 2 - CH_4, 3 - H_2 and 4 – CO, and a sharp increase in conversion of methane at 700℃. At the same time, syngas output will also increase. The carbonate conversion of methane at 800℃ and above reaches more than 80% yield. As a result of the increase in temperature during the conversion process, the yield of synthesis gas also increased at a temperature of 750-800°C.

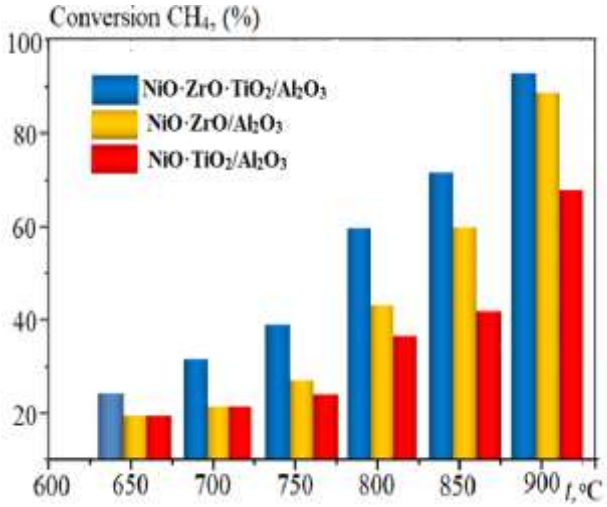

Figure 18. Histogram of Catalyst Usage in Methane Conversion

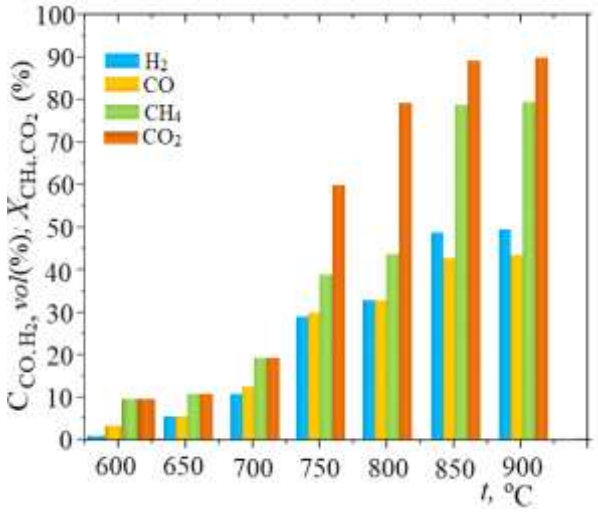

Figure 19. Histogram of the products formed during the conversion of carbonates

The effect of the synthesized catalysts on the carbonate catalytic conversion of methane at different temperatures was studied and their catalytic activity was evaluated (Fig. 18.19). In the process of methane conversion, the effect of the catalysts increases depending on the temperature. Among the catalysts, catalyst K3 can be considered as the catalyst, which has high catalytic activity. When using catalyst K3 at a temperature of 850-900°C, the efficiency of the catalytic conversion of methane is 73-97%. Accordingly, the conversion of methane increased with increasing temperature in both catalysts, the yield on catalyst K1 was 67–90%, and on catalyst K2, 45–70% at 850–900°C. This can be explained by the concentration of dopants in the catalyst.

Table 3 shows the results of carbonate conversion of methane and the conversion products for all three catalysts in the temperature range of 650-900℃, where the formation of a mixture of hydrogen, carbon monoxide (II) and carbon oxide (IV) is observed (Table 3).

Table 3. Results of the products formed from the carbonate conversion of methane

Catalysts	T, ℃	CH_4 conversion %	CO_2 conversion %	Formed product, %		
				H_2%	CO %	H_2:CO
K1	650°C	20	15	11,0	7,0	1,57:1
	700°C	23	19	13,0	9,3	1,4:1
	750°C	30	24	15	11,5	1,30:1
	800°C	47	39	23,2	18,3	1,27:1
	850°C	68	61	35,5	26,4	1,34:1
	900°C	87	77	47,9	33,9	1,41:1
K2	650°C	19	13	13,6	6,7	2:1
	700°C	22	17	16,4	12,5	1,31:1
	750°C	27	25	22,5	17,3	1,3:1
	800°C	40	37	33,7	24,2	1,39:1

	850°C	52	49	45,9	36,1	1,27:1
	900°C	71	65	53,8	45,8	1,17:1
K3	650°C	23	21	14,2	10,4	1,36:1
	700°C	36	33	27,6	23,8	1,16:1
	750°C	40	37	32,1	27	1,19:1
	800°C	65	62	48,5	42,6	1,14:1
	850°C	73	69	54,9	47,1	1,17:1
	900°C	92	87	57,6	51,9	1,11:1

It can be seen from the data in the table that at temperatures of 750-850°C, the values of methane conversion increased sharply and were average 35-70%. When the temperature increased to 900°C, the methane conversion rate exceeded 90%. It can bee seen that the conversion value increases with the amount of impurities in the catalyst. Figure 23 shows the dependence of CH_4/CO_2 ratio on the catalyst activity in the conversion process, and at a gas ratio close to or equal to 1:1, the conversion of methane and carbon dioxide is the highest, equal to 91.4.

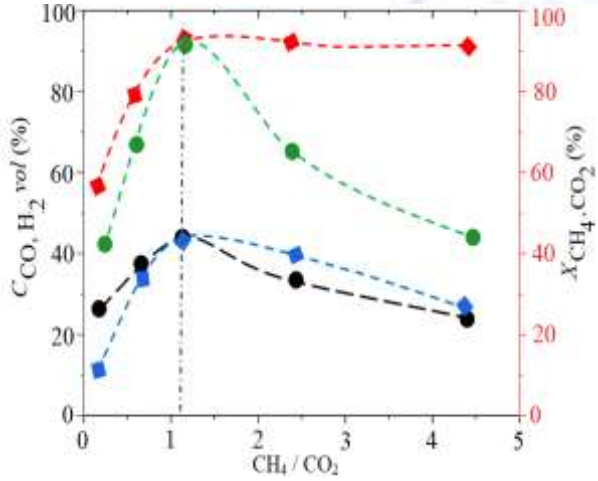

Figure 20. Effect of the ratio of CH_4/CO_2 gases on the catalyst activity

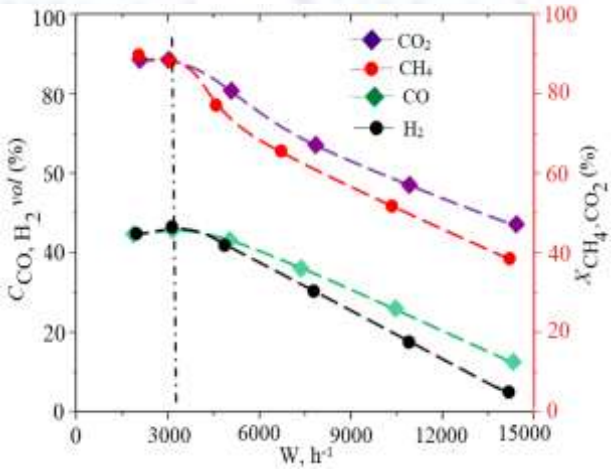

Figure 21. Effect of volume rate on the catalyst activity

In the conversion process, the most important is the ratio of gases, and the concentration of the resulting synthesis gas is achieved. At a ratio of initial products of 1:1, the yield of synthesis gas, that is, hydrogen and carbon monoxide (II), was maximum (H_2 - 43% and CO - 41%). An increase in the CH_4/CO_2 ratio causes a rather rapid decrease in the methane conversion. In contrast to methane, the carbon dioxide conversion ratio near 1 reached 92.3%, with a further increase to a plateau of 94%.

The dependence of the volume rate on the activity of the catalyst was also studied, and during the carbonate conversion, the values of the volume rate varied from 1450 h^{-1} to 3500 h^{-1}, a high degree of conversion and formation of the products were observed (Fig. 21). The conversion process was studied in the range from 1700 h^{-1} to 13000 h^{-1}, in this process the formation of products and the activity of the catalyst were observed.

3.3. Coking of the catalyst

Coking was studied by the method of X-ray diffractometry, the changes in phase composition and surface area, elemental analysis by SEM (Fig. 22, 23).

Composite catalyst K1 slightly changed its structure after catalytic investigations in the process of methane carbonate conversion. Only in some places new peaks were formed. As can be seen from the X-ray diffraction pattern, as a result of catalyst coking, a decrease in the intensity of its spectra is observed, as well as the formation of a new spectrum due to carbon (Fig. 22).

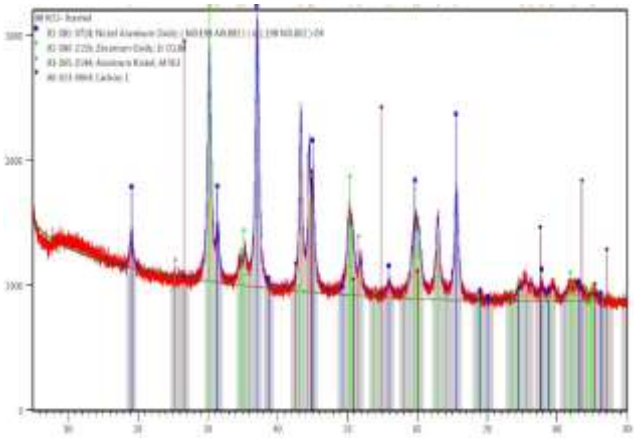

Figure 22. Diffractogram of K1 catalyst after conversion

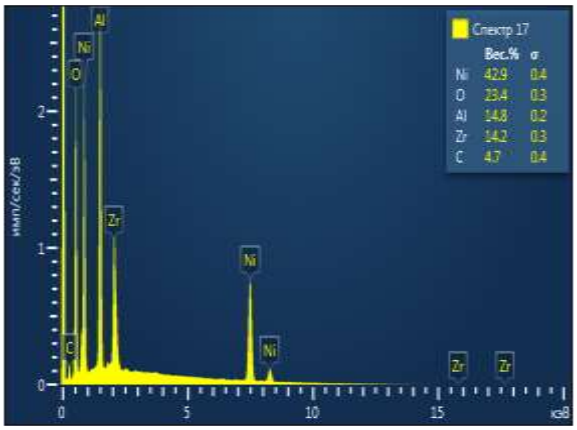

Figure 23. Element composition of K1 catalyst after conversion

According to the results of phase analysis, it became clear that a phase composition related to carbon was formed. First, if we analyze the changes in the phase composition as a result of coking of the composite catalyst K1: the initial phase composition contains NiO, aluminum-nickel oxide $NiAl_2O_4$ up to $ZrO_{1.88}$, and after conversion, nickel-aluminum oxide $(Ni_{0.198}Al_{0.802})$ $(Al_{1.198}NiO_{0.802})O_4$, zirconium oxide $ZrO_{1.88}$, $AlNi_3$ and C, as can be seen, form the phase composition.

According to the results of X-ray phase analysis, it can be concluded that due to the low level of coking on the catalyst surface, there was a very small change in the spectrum.

Elemental analysis on a scanning electron microscope (SEM) shows that the catalyst surface is coked to a certain extent, which is 4.7% of the total mass (Fig. 23). This is very small compared to the lifetime of the catalyst, which confirms the resistance of the catalyst to coking.

Changes in the spectra were analyzed by comparing the diffraction patterns of catalyst K1 before and after conversion (Fig. 24). In this case, partial changes occur in the X-ray spectra of catalyst K1, and the formation of new peaks can be observed due to the formation of coke on the catalyst surface.

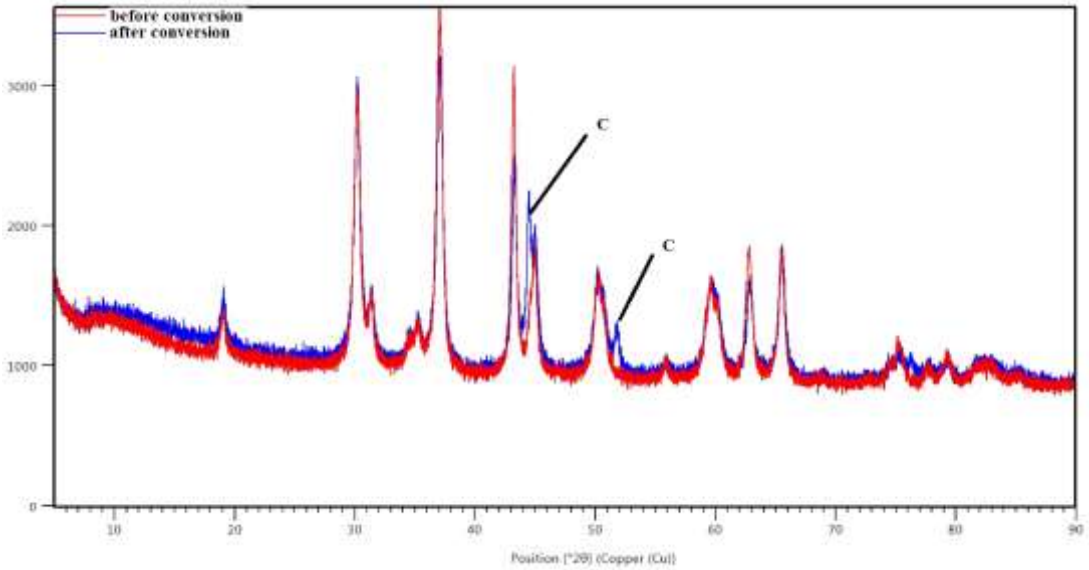

Figure 24. X-ray diffractograms of catalyst K1 before and after conversion

In addition, the elemental analysis after conversion shows that such regions mainly consist of carbon and nickel, therefore, the domains formed by the mutual combination of nickel and metal oxides used as dopants lead to coking of the catalyst surface (Fig. 28, 29).

After the conversion process, the effect of the coking process on the catalyst surface was studied using SEM microscopy. On Fig. 25a, the duration of the use of catalysts is 1700 h^{-1}, and in Figure 25b shows the results for 13000 h^{-1}. As it can be seen from the figures that the partial coking occurred only on the surface of the catalyst, which worked out for 1700 h^{-1} (Fig. 25a).

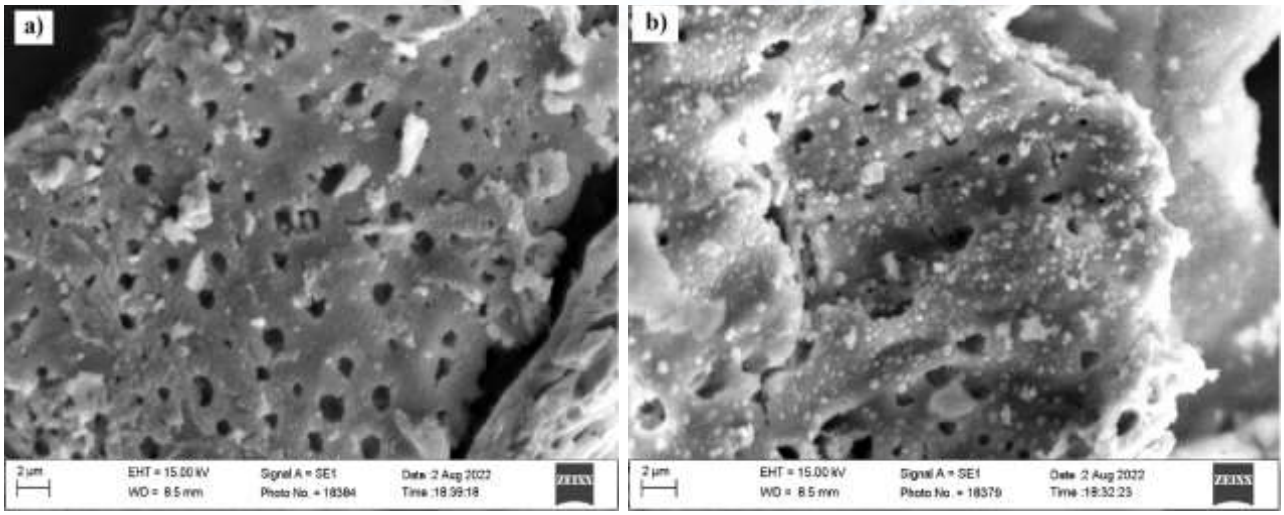

Figures 25 a,b. SEM image of composite catalyst K1 after conversion.

We can observe an increase in the amount of coking on the catalyst surface with increasing deposition time (Fig. 25b). In this case, the coarsening of carbon particles and more coking on the surface can be observed. The original surface structure has practically not changed. This is very small compared to the lifetime of the catalyst, which confirms the resistance of the catalyst to coking.

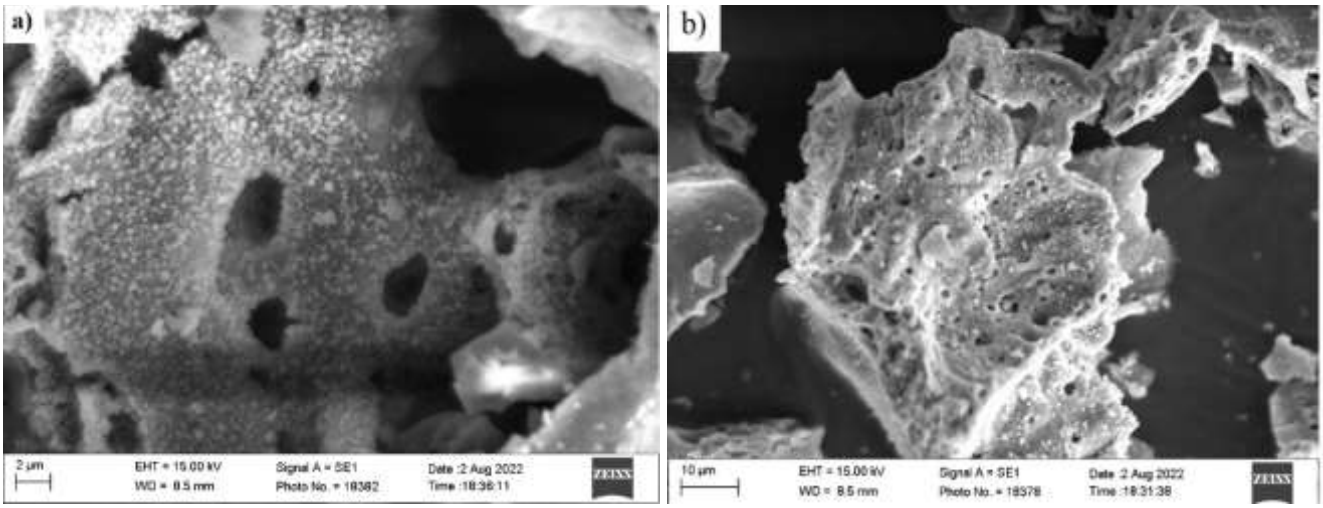

Figures 26 a,b. SEM image of composite catalysts K2 and K3 after conversion.

Coking of the surface of catalysts K2 and K3 was studied. In the images we can see small evenly coated particles on the surface of the catalyst, which are carbon particles. We see that carbon particles are only on the surface of the catalysts and are absent in the porous parts, that is, they have not completely covered the porous parts (Figures 26a,b). These data are also confirmed by elemental analysis produced by SEM (Fig. 27a,b).

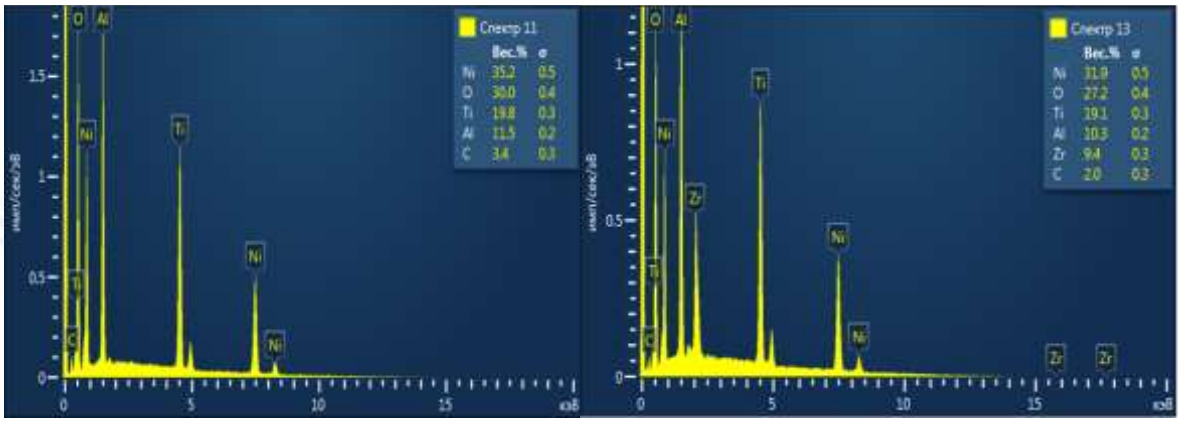

Figures 27 a,b. Element composition of catalysts K2 and K3 after conversion

In relation to the time of using composite catalysts K2 and K3 in the conversion process (13000hour^{-1}), the degree of coking is 2 ÷ 3.4 % of the total surface area, which is a very small part of the total amount. It makes the synthesized catalysts resistant to coking and possible for using in carbonate conversion.

CONCLUSIONS

1. The composite catalysts containing NiO were synthesized by the method of sol-gel "combustion solution synthesis" using $ZrO(NO_3)_2$ and $Ti(NO_3)_4$ as dopants based on some d-elements. It has been established that the phase composition of the prepared catalysts consists of NiO, $NiAl_2O_4$, $ZrO_{1.88}$, $Al_3Ni_2O_4$, TiO_2, Al_2O_3, $NiAl_2O_4$, $NiTiO_3$, $ZrO_{1.99}$, $(Al_3Ni_2)_{0.4}$, $Al_{16}Ni_7Ti_6$, $NiAl_3Zr_5$.
2. The sorption isotherms were studied by the adsorption of benzene and toluene vapors on catalysts, and some textural characteristics by SEM method. In accordance with that, the specific surface area

of the catalysts is S_{BET}= 420 ÷ 598 m^2/g, the specific pore volume V_s=0.74 ÷ 0.92 cm^3/g, the average pore diameter, D=220 ÷ 355 nm, the monolayer capacity a_m=0.96 ÷ 1.5 mol/kg and the saturation adsorption 2.2 ÷ 5.4 mol/kg.

3. The conversion of methane of 92% and carbon dioxide of 87% was achieved with the ratio of initial products of 1:1, an optimal temperature of 850-900℃, and a volume rate of 3000 h^{-1}. Under these conditions, the yield of hydrogen and CO was 57.6% and 51.9%.
4. When the application lifetime of the catalysts is 13,000 h^{-1} at conversion, the degree of coking was 2 ÷ 3.4% of the total surface area, which indicates the stability of the synthesized catalysts to coking

REFERENCES:

[1]. Saidov Kh.M.; Sayitkulov Sh.M.; Mukhamadiev N.K. Synthesis of the catalysts based on oxides of some d-elements. *Uzbek chemical journal*. **2019**; Volume 4, pp. 3-8 (in Uzbek).

[2]. Saidov Kh.M.; Mukhamadiyev N.K. Catalyst synthesis based on Ni, Zr oxides and its research. Int. Conf. on Integrated Innovative Development of Zarafshan Region: Achievement, Challenges and Prospects,Navoi, Uzbekistan, 27-28.11.2019; pp. 274-276.

[3]. Dossumov K.; Churina D.Kh.; Myltykbaeva L.K.; Tungatarova S.A. Oxide catalysts for hydrogen production from natural gas-methane in one stage. *European Applied Sciences*. 2013; Volume 7, pp. 92-94.

[4]. Lapidus A.L.; Zhagfarov F. G.; Sosna M.Kh.; Melnikov A.P.; Elkin A. B.; Chung Z. Study of the catalytic process of carbon dioxide conversion of natural gas. *Gas chemistry*. **2009**; Volume 3, pp. 14-26 (in Russian).

[5]. Cross A.; Roslyakov S.; Manukyan K.V.; Rouvimov S.; Rogachev A.S.; Kovalev D.; Mukasyan A.S. In situ preparation of highly stable Ni-based supported catalysts by solution combustion synthesis. *The Journal of Physical Chemistry*. **2014**; Volume 45, pp. 26191-26198.

[6]. Novikov V.; Xanthopoulou G.; Knysh Y.; Amosov A.P. Solution Combustion Synthesis of nanoscale Cu-Cr-O spinels: Mechanism, properties and catalytic activity in CO oxidation. *Ceramics International*, **2017**; Volume 15, pp 11733-11742.

[7]. Varma A.; Rogachev A.S.; Mukasyan A.S.; Hwang S. Combustion synthesis of advanced materials: principles and applications. *Advances in chemical engineering*, **1998**; Volume 24, pp 79-226

[8]. Stojanovic B.D.; Dzunuzovic A.S.; Ilic N.I. Review of methods for the preparation of magnetic metal oxides. *Magnetic, ferroelectric, and multiferroic metal oxides*, 2018; Elsevier, pp 333-359.

[9]. Li F. T.; Ran J.; Jaroniec M.; Qiao S.Z. Solution combustion synthesis of metal oxide nanomaterials for energy storage and conversion. *Nanoscale*, 2015; Volume 7. pp. 17590-17610.

[10]. Christy A.J.; Umadevi M.; Sagadevan S. Solution combustion synthesis of metal oxide nanoparticles for membrane technology. *Metal Oxide Powder Technologies*, 2020; Elsevier,. pp. 333-349.

[11]. Varma, A.; Mukasyan A.S.; Rogachev A.S.; Manukyan K.V. Solution combustion synthesis of nanoscale materials. *Chemical reviews*, **2016**; Volume. 116. pp. 14493-14586.

[12]. Wen W.; Wu J.M. Nanomaterials via solution combustion synthesis: a step nearer to controllability. *RSC advances*, **2014**. Volume. 4. pp. 58090-58100.

[13]. Harish V.; Tewari D.; Gaur M.; Yadav A.B.; Swaroop S.; Bechelany, M.; Barhoum A. Review on nanoparticles and nanostructured materials: Bioimaging, biosensing, drug delivery, tissue engineering, antimicrobial, and agro-food applications. *Nanomaterials*, **2022**. Volume. 12. pp 457.

[14]. Hossain M.K., Kecsenovity E., Varga A.; Molnar M.; Janáky C.; Rajeshwar; K. Solution combustion synthesis of complex oxide semiconductors. *International Journal of Self-Propagating High-Temperature Synthesis*, **2018**. Volume. 27. pp. 129-140.

[15]. Balamurugan S.; Linda Philip A.J.; Vidya R.S.A. Versatile combustion synthesis and properties of nickel oxide (NiO) nanoparticles. *Journal of Superconductivity and Novel Magnetism*, **2016**. Volume. 29. pp. 2207-2212.

[16]. Singhania A.; Krishnan V.V.; Bhaskarwar A.N.; Bhargava B.; Parvatalu D; Banerjee S. Hydrogen production from the decomposition of hydrogen iodide over nanosized nickel-oxide-zirconia catalysts prepared by solution-combustion techniques. *Catalysis Communications*. **2017**. Volume. 93. pp. 5-9.
[17]. Saidov Kh.M.; Mukhamadiev N.K. Synthesis of the catalysts based on oxides of some d-elements. *Scientific bulletin*. **2020**. pp. 58-60.
[18]. Saidov Kh.M.; Mukhamadiev N.K. Synthesis of the catalysts based on oxides of some d-elements .IOP Conference Series. *Materials Science and Engineering*. IOP Publishing **2020**. Volume. 1008. pp. 012035.
[19]. Khort A.; Hedberg J.; Mei N.; Romanovski V.; Blomberg E.; Odnevall I. Corrosion and transformation of solution combustion synthesized Co, Ni and CoNi nanoparticles in synthetic freshwater with and without natural organic matter. *Scientific reports*. **2021**. Volume. 11. pp. 1-14.
[20]. Li F. Solution combustion synthesis of metal oxide nanomaterials for energy storage and conversion. *Nanoscale*. **2015**. Volume. 7. pp. 17590-17610.
[21]. Saidov Kh.M.; Ruziev I.; Omontosheva M. T.; Mukhamadiev N.K. Synthesis of the catalysts based on oxides of some d-elements. Collection of articles of the III International Scientific and Practical Conference, Dushanbe, Tajikistan, 10.11.**2021**. pp. 28 – 32 (in Russian).
[22]. Kurzina I.A.; Godymchuk A.Yu.; Kachaev A.A. X-ray phase analysis of nanopowders . Tomsk: Tomsky Publishing House polytechnic university, Tomsk. Russia **2010**. pp.1-14.
[23]. Saidov Kh.M.; Sayitkulov Sh.M.; Mukhamadiev N.K. Study of the spatial composition of sorbents obtained from various soil samples using X-ray phase diffractometry. *Scientific Bulletin*. **2016**. Volume. 95 pp. 134-137 (in Uzbek).
[24]. Brożek-Mucha Z. Scanning electron microscopy and X-ray microanalysis for chemical and morphological characterisation of the inorganic component of gunshot residue: selected problems. *BioMed Research International*. **2014**. Volume. 2014 pp. 1-12.
[25]. Scapino L.; Zondag H.A.; Van Bael J.; Diriken J.; Rindt C.C. Sorption heat storage for long-term low-temperature applications: A review on the advancements at material and prototype scale. *Applied Energy*. **2017**. Volume. 190 pp. 920-948.
[26]. Kaumenova G.N. Development of Composite Materials by Combustion Synthesis for Catalytic Reforming of Methane into Hydrocarbons and Syngas . Dissertationб Phd, Kazakh National University named after. al-Farabiб Astana, Kazakhstan, **2020**. (in Russian).
[27]. Monroy T. G.; Abella L.C.; Gallardo S.M.; Hinode H. Catalytic dry reforming of methane using Ni/MgO-ZrO_2 catalyst. *Proceedings of the and Annual Gas Processing Symposium*. Elsevier, **2010**. pp. 145-152.
[28]. Khan H.; Yerramilli A.S.; D'Oliveira A.; Alford T.L.; Boffito D.C.; Patience G.S. Experimental methods in chemical engineering: X- ray diffraction spectroscopy—XRD. *The Canadian Journal of Chemical Engineering*. **2020**. Volume. 98. pp. 1255-1266.
[29]. Singh S.D.; Nand M.; Das A.; Ajimsha R.S.; Upadhyay A.; Kamparath R.; Ganguli. Structural, electronic structure, and band alignment properties at epitaxial NiO/Al_2O_3 heterojunction evaluated from synchrotronbased X-ray techniques. *Journal of Applied Physics*. **2016**. Volume. 119. pp. 165302.
[30]. Uzokov J.R.; Mukhamadiev N.K. Sorption characteristics of mesoporous composite $SiO_2 \cdot TiO_2$. *Central asian journal of medical and natural sciences*. **2021**. Volume. 2. pp. 494-498.
[31]. Hernández M.A.; Velasco J.A.; Asomoza M.; Solis S.; Rojas F.; Lara V.H. Adsorption of benzene, toluene, and p-xylene on microporous SiO_2. *Industrial and engineering chemistry research*. **2004**. Volume. 43. pp. 1779-1787.
[32]. Uzokov J.R.; Mukhamadiev N.K. Sorption Characteristics of The Mesoporous Sorbents Based On Tetraethoxysilane And Titanium Oxide. *European Journal of Molecular & Clinical Medicine*. **2020**. Volume. 7. pp. 656-660.
[33]. Kotkowski T.; Cherbański R.; Molga E. Tyre-derived activated carbon–textural properties and modelling of adsorption equilibrium of n-hexane. *Chemical and Process Engineering*. **2020**. Volume. 41. pp. 25–44.

[34]. Abbas S. Z.; Dupont V.; Mahmud T. Kinetics study and modelling of steam methane reforming process over a NiO/Al_2O_3 catalyst in an adiabatic packed bed reactor. *International journal of hydrogen Energy*. **2017**. Volume. 42. pp. 2889-2903.

[35]. Li H.; Xu H.; Wang J. Methane reforming with CO_2 to syngas over CeO_2-promoted Ni/Al_2O_3-ZrO_2 catalysts prepared via a direct sol-gel process. *Journal of natural gas chemistry*. **2011**. Volume. 20. pp. 1-8.

[36]. Al-Fatesh A.; Singh S.K.; Kanade G.S.; Atia H.; Fakeeha A.H.; Ibrahim A.A.; Labhasetwar N.K. Rh promoted and ZrO_2/Al_2O_3 supported Ni/Co based catalysts: High activity for CO_2 reforming, steam–CO_2 reforming and oxy–CO_2 reforming of CH_4. *International journal of hydrogen energy*. **2018**. Volume. 43. pp. 12069-12080.

[37]. Sakamoto K.; Hayashi F.; Sato K.; Hirano M.; and Ohtsu, N. XPS spectral analysis for a multiple oxide comprising NiO, TiO_2, and $NiTiO_3$. *Applied Surface Science*. **2020**. Volume. 526. pp. 146729.

[38]. Hosseinpour-Mashkani S.M.; Maddahfar M.; Sobhani-Nasab A. Novel silver-doped $NiTiO_3$: auto-combustion synthesis, characterization and photovoltaic measurements. *South African Journal of Chemistry*. **2017**. Volume. 70. pp. 44-48.

[39]. Tamimi K.; Alavi S. M.; Rezaei M.; Akbari E.I. Preparation of the Mn-Promoted NiO–Al_2O_3 nanocatalysts for low temperature CO_2 methanation. *Journal of the Energy Institute*. **2021**. Volume. 99. pp. 48-58.

[40]. Alawi N.M.; Barifcani A.; Abid H.R. Optimisation of CH_4 and CO_2 conversion and selectivity of H_2 and CO for the dry reforming of methane by a microwave plasma technique using a B ox–B ehnken design. *Asia-Pacific Journal of Chemical Engineering*. **2018**. Volume. 13. pp. 2254.

[41]. Soloviev S.O.; Kapran A. Y.; Orlyk S.N.; Gubareni E.V. Carbon dioxide reforming of methane on monolithic Ni/Al_2O_3-based catalysts. *Journal of natural gas chemistry*. **2011**. Volume. 20. pp. 184-190.

[42]. Liu H. CO_2 Chemical Utilization through Dry Reforming of Methane: Development of Non-Noble Metals Catalysts Supported on Natural and Synthetic Clays. dis, PhD, Sorbonne université, Paris, France, **2018**.

[43]. Burger T. COx Methanation over Ni-Al-Based Catalysts: Development of CO_2 Methanation Catalysts and Kinetic Modeling. dis, PhD, Technical university of Munich, Munich, Germany. **2021**. (in German)

[44]. Pashchenko D. Experimental investigation of synthesis gas production by methane reforming with flue gas over a NiO-Al_2O_3 catalyst: Reforming characteristics and pressure drop. *International Journal of Hydrogen Energy*. **2019**. Volume. 44.pp. 7073-7082.